

UC San Diego

UC San Diego Previously Published Works

Title

Computer-aided drug design guided by hydrogen/deuterium exchange mass spectrometry: A powerful combination for the development of potent and selective inhibitors of Group VIA calcium-independent phospholipase A2

Permalink

<https://escholarship.org/uc/item/2sw9b1r3>

Journal

Bioorganic & Medicinal Chemistry, 24(20)

ISSN

0968-0896

Authors

Mouchlis, Varnavas D
Morisseau, Christophe
Hammock, Bruce D
[et al.](#)

Publication Date

2016-10-01

DOI

10.1016/j.bmc.2016.05.009

Peer reviewed



HHS Public Access

Author manuscript

Bioorg Med Chem. Author manuscript; available in PMC 2017 October 15.

Published in final edited form as:

Bioorg Med Chem. 2016 October 15; 24(20): 4801–4811. doi:10.1016/j.bmc.2016.05.009.

Computer-Aided Drug Design Guided by Hydrogen/Deuterium Exchange Mass Spectrometry: A Powerful Combination for the Development of Potent and Selective Inhibitors of Group VIA Calcium-Independent Phospholipase A₂

Varnavas D. Mouchlis^{†,*}, Christophe Morisseau[‡], Bruce D. Hammock[‡], Sheng Li[§], J. Andrew McCammon^{†,*}, and Edward A. Dennis^{†,*}

[†]Department of Pharmacology and Department of Chemistry and Biochemistry, School of Medicine, University of California, San Diego, La Jolla, California 92093-0601, USA

[‡]Department of Entomology and Nematology and UC Davis Comprehensive Cancer Research Center, University of California, Davis, CA 95616, USA

[§]Department of Medicine, University of California, San Diego, La Jolla, California 92093-0601, USA

Abstract

Potent and selective inhibitors for phospholipases A₂ (PLA₂) are useful for studying their intracellular functions. PLA₂ enzymes liberate arachidonic acid from phospholipids activating eicosanoid pathways that involve cyclooxygenases (COX) and lipoxygenases (LOX) leading to inflammation. Anti-inflammatory drugs target COX and LOX; thus, PLA₂ can also be targeted to diminish inflammation. This paper describes the employment of enzymatic assays, hydrogen/deuterium exchange mass spectrometry (DXMS) and computational chemistry to develop PLA₂ inhibitors. Beta-thioether trifluoromethylketones (TFKs) were screened against human GVIA calcium-independent, GIVA cytosolic and GV secreted PLA₂s. These compounds exhibited inhibition towards Group VIA calcium-independent PLA₂ (GVIA iPLA₂), with the most potent and selective inhibitor **3** (OTFP) obtaining an X₁(50) of 0.0002 mole fraction (IC₅₀ of 110 nM). DXMS binding experiments in the presence of OTFP revealed the peptide regions of GVIA iPLA₂ that interact with the inhibitor. Molecular docking and dynamics simulations in the presence of a membrane were guided by the DXMS data in order to identify the binding mode of

*Corresponding Authors V.D.M.: vmouchlis@gmail.com, J.A.M.: jmccammon@ucsd.edu, E.A.D.: edennis@ucsd.edu; phone, +1 858 534 3055.

Publisher's Disclaimer: This is a PDF file of an unedited manuscript that has been accepted for publication. As a service to our customers we are providing this early version of the manuscript. The manuscript will undergo copyediting, typesetting, and review of the resulting proof before it is published in its final citable form. Please note that during the production process errors may be discovered which could affect the content, and all legal disclaimers that apply to the journal pertain.

Supplementary Material

Additional figures (PDF).

3D movies for MD simulation on GVIA iPLA₂-OTFP complexe (mpg):

Movie 1: GVIA iPLA₂-OTFP complex

Movie 2: H-bonds of fluoroketone group and sulfur atom

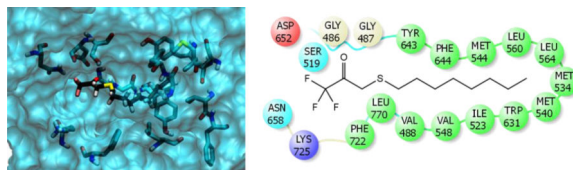
Movie 3: Pi-Pi stacking of sulfur atom

Data of Table 1 (CSV)

Data of Table 3 (CSV)

OTFP. Clustering analysis showed the binding mode of **OTFP** that occurred 70% during the simulation. The resulted 3D complex was used for docking studies and a structure-activity relationship (SAR) was established. This paper describes a novel multidisciplinary approach in which a 3D complex of GVIA iPLA₂ with an inhibitor is reported and validated by experimental data. The SAR showed that the sulfur atom is vital for the potency of beta-thioether analogues, while the hydrophobic chain is important for selectivity. This work constitutes the foundation for further design, synthesis and inhibition studies in order to develop new beta-thioether analogues that are potent and selective for GVIA iPLA₂ exclusively.

Graphical Abstract



Keywords

Phospholipase A₂; trifluoromethylketones; thioether; DXMS; docking; MD simulations; structure-activity relationship

1. Introduction

Phospholipase A₂ (PLA₂) constitutes a superfamily of enzymes that is implicated in many biological pathways because of its unique ability to catalyze the hydrolysis of the ester bond at the *sn*-2 position of membrane phospholipid molecules [1, 2]. The products of their catalytic action include arachidonic acid (AA) and other free fatty acids as well as lysophospholipids (LP). AA and LP are metabolic precursors of numerous metabolites involved in inflammatory conditions including prostaglandins (PG), leukotrienes (LT), and platelet-activating factor (PAF) [3-5]. The PLA₂ family includes six main types: cytosolic (cPLA₂), secreted (sPLA₂), calcium-independent (iPLA₂), platelet-activating factor acetylhydrolase (PAF-AH) also referred to as lipoprotein-associated phospholipase A₂ (Lp-PLA₂), lysosomal phospholipase A₂ (L-PLA₂), and adipose-PLA₂ (AdPLA) [1]. During the last decade, it has been shown that PLA₂s are associated with several inflammatory diseases including asthma, arthritis, and cancer, and thus constitute an attractive target for inhibitor development [6-8].

Among the PLA₂ enzymes, the Group VIA calcium-independent PLA₂ (GVIA iPLA₂ also known as PNPLA9) has attracted considerable pharmaceutical interest because it is implicated in many diseases including diabetes [9], Barth syndrome [10], and NBIA/ Neuroaxonal Dystrophy [11], and thus, the development of potent inhibitors that are also highly selective for GVIA iPLA₂ may lead to new therapeutics. The association of GVIA iPLA₂ with membranes and the lack of an X-ray crystal structure to assist *in silico* design render the developments of inhibitors very challenging. The human GVIA iPLA₂ gene was found to express multiple splice variants, with transcript variant 1 to be one of the two active

isoforms in humans. Splice variant 1 contains 806 amino acids, and a molecular weight of 90 kDa. Based on its sequence, GVIA iPLA₂ is composed of 7 ankyrin repeats, a linker region that contains an insert of 54 amino acids disrupting the eighth ankyrin repeat, and a patatin-like α/β hydrolase catalytic domain. The enzyme belongs to the carboxylesterase family that utilizes a catalytic dyad of Ser/Asp instead of the conventional carboxylesterase catalytic triad of Ser/His/Glu or Asp [1]. Even though there is no available crystal structure for GVIA iPLA₂, molecular docking and dynamics (MD) simulations guided by hydrogen/deuterium exchange mass spectrometry (DXMS) data have successfully been used in the past by our group, to study the interactions of a GVIA iPLA₂ homology model with membranes, substrates and inhibitors [12-14].

Several compounds have been reported to inhibit the enzymatic activity of GVIA iPLA₂ including the *S*-enantiomer of the historically used covalent inhibitor bromoenol lactone (*S*-BEL) [15]. Although BEL potently inhibits the enzyme, it has low selectivity because it also inhibits other serine proteases. Methyl arachidonyl fluorophosphonates (MAFP) are also potent GVIA iPLA₂ inhibitors, but they are irreversible, and not specific for iPLA₂ [16]. Another class of GVIA iPLA₂ inhibitors is the 2-oxoamides based on dipeptides and pseudo dipeptides, but they also inhibit cPLA₂ [17]. In 1995, fatty acyl trifluoromethylketones (TFKs) were identified as promising GVIA iPLA₂ inhibitors that target the catalytic Ser [15]. Further, development of various polyfluoroketones by Kokotos *et al* led to a series of small aromatic compounds as potent and selective inhibitors of human GVIA iPLA₂ [18, 19].

TFKs are well known in mammalian pharmacology, and they were reported as transition state esterase inhibitors [20, 21]. They were also found to be potent inhibitors of an insect juvenile hormone esterase [22]. Thioether TFK analogues were found to be 10-50 times more potent [23] and active *in vivo* to disrupt insect development [24]. However, these analogues were not extensively studied in mammalian enzymes compared to the non-thioether ones. The first mammalian enzyme that the beta-thio TFKs were found to be potent as inhibitors is carboxylesterase, which also exhibited an increased potency over the non-thio TFKs [25-28]. In spite of multiple studies and X-ray structures of the thio TFKs in esterase catalytic sites, the exact contribution of the thioether to inhibitor potency remains elusive [29]. The sulfur atom was initially added into TFKs as a bioisosteric replacement of the olefin group in juvenile hormone and it increased the efficacy of TFKs greater than expected. It is well known that the carbonyl group in TFKs exists in equilibrium with the hydrate (gem diol) form, because the polarization of the ketone is enhanced by the fluorine atoms [30, 31]. One of the hypotheses related to the increased efficacy of the thio TFKs is that the sulfur atom shifts the equilibrium towards the gem diol form [32]. An alternative hypothesis is that the sulfur atom may participate in π -stacking interactions with aromatic residues in the enzyme active site [26].

In this study a series of beta-substituted TFKs containing a sulfur, oxygen and selenium atom at the beta-carbon atom were tested towards human Group VIA calcium-independent, Group IVA cytosolic and Group V secreted PLA₂. TFKs were previously synthesized by Hammock's group and were initially tested toward juvenile hormone esterase and mammalian carboxylesterases [26, 27]. Beta-thio TFKs exhibited inhibition against GVIA

iPLA₂ while they don't show significant activity towards GIVA cPLA₂ and GV sPLA₂. The most potent and selective inhibitor **3** (**OTFP**) exhibited an X_I(50) of 0.0002 mole fraction corresponding to IC₅₀ of 110 nM. In the absence of a crystal structure for GVIA iPLA₂, DXMS was employed to identify the peptide regions of GVIA iPLA₂ showing decreased deuteration levels upon binding with the **OTFP**. The DXMS data were used to guide molecular docking and dynamics (MD) simulations in the presence of a POPC membrane patch. Clustering analysis led to an enzyme-inhibitor complex that revealed a detailed binding mode of **OTFP** in the enzyme binding site. This binding mode occupies 70% of the binding modes occurring during the MD simulation. The resulted 3D complex was used to dock all the compounds with X_I(50) values and the established SAR model exhibited very good linearity between the theoretical binding score (XP GScore) and the experimental inhibitory activity (r² of 0.8). The docking complexes provide insight into the structure-activity relationship (SAR) that will be used to design, synthesize and test new beta-thioether analogues in order to identify compounds with improved inhibitory properties against GVIA iPLA₂. This work represents a novel multidisciplinary approach showing that the combination of computer-aided design along with experimental techniques is a powerful tool in drug discovery.

2. Results and Discussion

2.1. Inhibition of human GVIA iPLA₂, GIVA cPLA₂ and GV sPLA₂

Trifluoromethylketones (TFKs) were tested for their inhibitory activity against the human recombinant PLA₂ enzymes using a mixed micelle modified Dole assay [33, 34]. Table 1 summarizes the structure and inhibitory activity of TFKs towards three human PLA₂ enzymes. Initial screening was performed for each PLA₂ enzyme at 0.091 mole fraction of the compound in the total surface volume of the mixed micelles, and then the X_I(50) was determined for the compounds that exhibited more than 95 % inhibition. An exception was made for compound **1** because it was used for the SAR. X_I(50) is defined as the mole fraction of the compound in the total PAPC substrate/Triton X-100 mixed micelle surface required to inhibit 50% of the enzyme [33]. Mole fraction is a dimensionless number derived by dividing the number of moles of inhibitor by total number of moles of substrate plus inhibitor plus detergent. X_I(50) values can be converted to molar concentration by considering that 0.091 mole fraction of inhibitor corresponds to a 50 μM concentration. Thus, an X_I(50) of 0.0002 corresponds to 110 nM.

Among the TFKs containing an aliphatic chain (**1-6**, Table 1) compound **3** (**OTFP**), which contains eight carbon atoms in its aliphatic chain, exhibited the highest inhibition against GVIA iPLA₂ (see sigmoidal response curve in Fig. S1), while it did not show significant inhibition towards GIVA cPLA₂ and GV sPLA₂. When the number of carbon atoms of the aliphatic chain was decreased by two in compound **2**, the activity against GVIA iPLA₂ was also reduced by twofold. Further decrease of the number of carbon atoms by four in compound **1** reduced the inhibitory activity by two orders of magnitude. Increasing the carbon atoms of the aliphatic chain by two in compound **4** and three in compound **5** reduced the inhibitory activity against GVIA iPLA₂ by 1.5 and 2.5-fold, respectively, while the two compounds also lost selectivity since they also inhibited GIVA cPLA₂, even though their

inhibitory activity against GIVA cPLA₂ was one and two orders of magnitude, respectively, less in comparison with GVIA iPLA₂. Further increases in the number of carbon atoms of the aliphatic chain by four in compound **6** reduced the inhibitory activity against GVIA iPLA₂ by one order of magnitude. According to the above results, the size of the aliphatic chain is crucial for the potency and selectivity of these inhibitors against GVIA iPLA₂ with the optimum number of carbon atoms being eight in compound **3** (**OTFP**). Thus, by optimizing the hydrophobic chain of beta-thio TFKs, it is possible to improve potency and selectivity toward GVIA iPLA₂ versus GIVA cPLA₂ since these properties depend on the size of the hydrophobic chain.

Compounds **7-17** contain an aromatic ring in the hydrophobic chain (Table 1). Compounds **7-15** contain a phenyl group directly connected to the sulfur atom and they exhibited similar inhibition against GVIA iPLA₂, except for compound **13** which contains a polar nitro group on the phenyl ring. Slight differences in the inhibitor activity towards GVIA iPLA₂ depend on the position of the various substitutions on the phenyl ring, while none of them significantly inhibits GIVA cPLA₂ and GV sPLA₂. Compound **16** (**PETFP**), which contains two extra carbon atoms between the sulfur atom and the phenyl ring exhibited the highest inhibitory activity among this set of compounds. It is worth mentioning that the inhibitory activity of **PETFP** is almost the same as the one exhibited by compound **2** and two-fold less than the inhibitory activity of **OTFP**. **PETFP** and **2** have similar sizes since the number of carbon atoms from the sulfur atom to the end of the chain is six. The above results support further the notion that by optimizing the hydrophobic chain of beta-thio TFKs, it is possible to alter potency and selectivity towards GVIA iPLA₂. Finally, it seems that the sulfur atom plays an important role on the inhibitory activity of these compounds because compound **17** which contains a selenium atom showed insignificant activity. While the size of the hydrophobic chain plays a significant role in the selectivity of beta-thio TFKs, it is clear that the sulfur atom is vital for the potency of these analogues. Thus, altering the beta-thioether and the hydrophobic chain can be consider important tools in designing new more potent and selective analogues.

Compounds **18-26** are variously substituted-TFKs. Compound **18** that contains an oxygen atom exhibited an order of magnitude less inhibitory activity against GVIA iPLA₂ than its sulfur analogue **2** showing the importance of the sulfur atom for the potency of these compounds. Compound **19** showed very low activity towards GVIA iPLA₂ indicating the importance of the carbonyl group for the inhibitory activity of these compounds. Compounds **20-26** contain various substitutions of the sulfur atom and the carbonyl group and none of them exhibited significant inhibition against any of the three PLA₂ groups, further supporting the necessity of the sulfur atom and the carbonyl group for the inhibitory activity of TFKs.

2.2. Defining the binding site of OTFP using DXMS

Hydrogen/deuterium exchange mass spectrometry (DXMS) [35] is a powerful technique used to study the structural dynamics of membrane proteins [36, 37] as well as the association of PLA₂ enzymes with membranes [38, 39]. With DXMS we are able to capture the exchange rates of the backbone amide hydrogen atoms of an enzyme with deuterium

atoms after incubation of the enzyme with deuterium dioxide. This method was successfully combined with computational methods to study the interactions of PLA₂ enzymes with membranes, substrates and inhibitors [12, 14, 40]. The combination of DXMS experimental data with molecular docking and dynamics simulations has been proven very powerful in elucidating the binding mode of **OTFP** in the binding site of GVIA iPLA₂ considering that the X-ray crystal structure of the enzyme has not been solved yet.

2.3. Digestion Map of GVIA iPLA₂

The enzyme digestion was optimized to give a peptide map with the highest coverage of GVIA iPLA₂ sequence as previously described [14]. The optimized condition yielded 174 distinct peptides that gave 90% coverage of the GVIA iPLA₂ sequence (Fig. S2). Among these peptides, 70 peptides with the best signal-to-noise ratio were used for the analysis.

2.4. Interactions of OTFP with GVIA iPLA₂ binding site

According to the inhibition studies **OTFP** is a competitive reversible inhibitor (sigmoidal response curve, Fig. S1). As a result, deuteration changes upon **OTFP** binding were expected around the binding site of GVIA iPLA₂. In particular, seven peptide regions surrounding the binding site, residues 481-493 (yellow), 514-524 (magenta), 542-562 (orange), 630-655 (green), 656-664 (pink), 718-730 (red), and 770-778 (blue) in Fig. 1, exhibited the most significant decrease of deuteration levels (Table 2). None of these peptides showed an increase in deuteration after the binding experiment with **OTFP**. Region 481-493 in the absence of **OTFP** showed an average of 43% deuteration, while in the presence of **OTFP** showed a 27% deuteration which is a decrease of approximately 16%. This region contains the oxyanion hole (Gly486/Gly487) that stabilizes the tetrahedral intermediate during the hydrolysis of a phospholipid substrate [12]. Region 542-562 contains the catalytic serine (Ser519), and showed an average decrease of 13% deuteration in the presence of **OTFP**. Region 630-655 contains the catalytic aspartic acid (Asp652), and showed a decrease of approximately 12% deuteration in the presence of **OTFP**. Regions 656-664 and 718-730 are located near the catalytic aspartic acid (Asp652), and they showed an average decrease of 12% and 13% deuteration in the presence of **OTFP**, respectively. These regions contain residues like Asn658 and Lys725 that might interact with the fluorine atoms of **OTFP**. Peptide region 718-730 is part of the membrane anchor region 708-730 that was found to show more than 40% decrease in deuteration rates in the presence of PAPC vesicles [38]. Using coarse-grained and atomistic MD simulations, we have elucidated the association mechanism of this region with the membrane [13]. It is worth mentioning that in the presence of the **OTFP** inhibitor part of the same region (residues 718-730) showed only 13% decrease of deuteration level. Finally, regions 542-562 and 770-778 contain mostly hydrophobic residues that might interact with the alkyl chain of **OTFP**, and they both showed a significant decrease of deuteration level in the presence of the inhibitor (18% and 20%, respectively).

2.5. Binding mode of OTFP in GVIA iPLA₂ binding site

The binding mode of **OTFP** was calculated computationally using the homology model of GVIA iPLA₂ [12] and the Induced Fit Docking (IFD) protocol implemented in Schrödinger

suite [41]. Residues Gly486, Gly487, Lys489, Ser519, Val548, Phe549, Leu560, Tyr643, Phe644, Asp652, Lys729, and Leu770 were selected to define the binding site of GVIA iPLA₂ in the IFD calculations. These residues exhibited significant decreased percentage of deuteration levels in DXMS studies upon binding of **OTFP** inhibitor (see DXMS results). According to the 3D GVIA iPLA₂-**OTFP** complex generated by IFD (Fig. 2A) the trifluoromethylketone group is located in the hydrophilic region of GVIA iPLA₂ binding site with the oxygen atom of the carbonyl group participating in one hydrogen bond (H-bond) with the catalytic Ser519. The fluorine atoms are in spatial proximity with residues Asn658 and Lys725. The alkyl chain of the inhibitor is accommodated near the entrance of the binding site interacting with residues such as Val548, Phe549, Leu560, Tyr643, Phe644, and Leu770.

The GVIA iPLA₂-**OTFP** IFD complex was placed on the surface of a POPC membrane patch (Fig. 3), solvated with explicit water molecules, minimized, equilibrated and subjected to a 300 ns simulation using NAMD 2.9 [42]. The structural stability of the complex was indicated by a stable root mean square deviation (RMSD) of the backbone atoms aligned to the GVIA iPLA₂-**OTFP** IFD complex, which was stabilized at ~2.3 Å showing that the simulation was reasonably converged (Fig. S3). Figure 2B and Movie 1 shows the binding mode of **OTFP** after the MD simulation. In the hydrophilic area of the binding site the oxygen atom of the carbonyl group participates in H-bonding with residues Gly486/Gly487 the so called “oxyanion hole”. The distances between H-bond acceptor and donor are ~3 Å after the first 150 ns of the simulation and until the end (Fig. S4A). Movie 2 shows the interactions of the fluoroketone group occur during the simulation. The catalytic Ser519 does not form any H-bonds with the carbonyl group even if they are in spatial proximity (~3 Å after the first 150, Fig. S4A), because the hydrogen atom of the hydroxyl group doesn't adopt a suitable orientation to form an H-bond (Movie 2). Ser519 constantly forms H-bonding with the catalytic Asp652 (Movie 2). It has been argued for years that TFKs exist in equilibrium between the ketone and the hydrate form. It is possible that fluorine and sulfur atoms shift the equilibrium in favor of the hydrate form, however, the ketone is considered to be the reactive form of the inhibitor, which might undergoes nucleophilic attack by the hydroxyl group of catalytic serine (Ser519-OH) [27]. During the simulations the oxygen atom of the carbonyl group is constantly interacting with the “oxyanion hole” (Gly486/Gly487), while the carbon atom of the carbonyl group is very close to catalytic Ser519 suggesting that its hydroxyl group is in spatial proximity to form a reversible hemiketal (Movie 2). It is likely that the hemiketal is stabilized by the “oxyanion hole” (Gly486/Gly487), however, no one has been able to definitively show that the carbonyl group forms a hemiketal with the catalytic serine. The fluorine atoms interact with Asn658 (~3.3 Å, Fig. S4A) but no interactions were observed with Lys725 (Movie 2).

The alkyl chain moves from the entrance into the hydrophobic region of the binding site (Movie 1). Clustering analysis revealed that 70% of the snapshots saved in the MD trajectory show the hydrophobic chain of **OTFP** in a horizontal (Fig. 2B and Movie 1), rather than a vertical orientation suggested by IFD (Fig. 2A). The simulation showed the hydrophobic chain to interact with residues like Val488, Ile523, Tyr541, Met544, Val548, Phe549, Leu560, Tyr643, Phe644 and Leu770 (Movie 1). Our previously published work

showed that the same hydrophobic region is occupied by the *sn*-2 fatty acyl chain of a PAPC substrate molecule [12]. The sulfur atom is in spatial proximity with Gly487 (~3.9 Å acceptor-donor distance, Fig. S4B) which is part of the “oxyanion hole” suggesting the formation of a weak H-bond (Movie 2). Two aromatic residues, Tyr643 and Phe722 are also located near the sulfur atom competing for pi-pi stacking interactions (Movie 3). The distance of the phenyl ring centroid of Tyr643 is ~4 Å and is increasing to ~5 Å when the phenyl ring of Phe722 is approaching the sulfur atom (Fig. S4B). Sulfur is a highly versatile atom in terms of the molecular interactions that it can form in molecular recognition. It has the ability to interact with electron-poor and with electron-rich functional groups [43]. The backbone amide hydrogen atom of Gly487 is electron-poor, while the aromatic rings of Tyr643 and Phe722 are electro-rich because of their π electron cloud and it is possible that the sulfur atom is involved in interactions with these residues (Movie 2 and 3). This observation is in agreement with the hypothesis suggested by Wheelock and his coworkers that the sulfur atom enhances the efficacy of TFKs because is involved in π -stacking interactions with aromatic residues of the active site [26].

2.6. Structure-activity relationship (SAR)

Five representative enzyme-inhibitor complexes were chosen from the five clusters resulted from the clustering analysis for docking calculations. These complexes were optimized using the Protein Preparation Wizard (PPW) [44] and the **OTFP** inhibitor was redocked into the GVIA iPLA₂ binding site using Glide [45]. The complex that received the highest XP GScore (Extra-Precision Glide Score) and was used to perform docking calculations on the set of 14 inhibitors for which $X_1(50)$ values were measured. The theoretical binding scores (Table 3) were correlated with $-\log X_1(50)$ values and an $r^2=0.8$ suggested very good correlation between theoretical and experimental results (Fig. 4).

The SAR model suggests that docking calculations can be used to predict the potency of these compounds towards GVIA iPLA₂. It should be noted that compounds with high $X_1(50)$ values tend to have higher XP GScore, while compounds with low $X_1(50)$ values tend to have a lower XP GScore within the acceptable error that is typical for docking calculations. In addition to the predictions of the binding score, the docking 3D complexes provide insight into the binding mode of these compounds. According to the docking complex, **OTFP** has the suitable size to fit into the binding site of GVIA iPLA₂ and optimize its binding exhibiting the higher inhibition against the enzyme (Fig. 4 and Table 3). **PETFP** and **2** lack interactions with the hydrophobic pocket of GVIA iPLA₂ due to shorter hydrophobic chains therefore their inhibition against the enzyme is 30-fold less than **OTFP**. The aliphatic chains of **2** and **18** are identical showing similar interactions with the hydrophobic region of the enzyme binding site. However, inhibitor **18** exhibited 12-fold less inhibition than inhibitor **2** due to replacement of the sulfur atom by an oxygen atom. The oxygen atom is smaller and its electron cloud is not as extended as the one of the sulfur atom resulting in weaker interactions of the oxygen atom with the aromatic residues of the binding site. The non-thio derivative of **PETFP** was previously tested and published as a GVIA iPLA₂ inhibitor with an $X_1(50)$ of 0.0096 [46]. **PETFP** exhibited 16-fold higher inhibition than its non-thio derivative. These two examples clearly indicate the significant role of the sulfur atom in improving the inhibitory potency of these compounds. Finally, the lower inhibition

of **4** and **5** in comparison with **OTFP** indicating that eight is the optimum number of carbon atoms for the hydrophobic chain. Increases in the hydrophobic chain length results in weaker binding, probably due to steric clashes with the residues of the hydrophobic region in the enzyme binding site.

The docking calculation also revealed important information for the selectivity of these compounds. Inhibitor **OTFP**, **4**, and **5** were docked in the binding site of GIVA cPLA₂ (Table 3 and Fig. 5). **OTFP** received lower XP GScore than inhibitors **4** and **5** but most importantly the docking complexes showed that the deep channel-like binding site of GVIA cPLA₂ requires longer hydrophobic chains for optimum binding of the inhibitor with ten being the optimum number of carbon atoms in inhibitor **4**. The hydrophobic chain of inhibitor **4** and **5** is accommodated in GIVA cPLA₂ more favorably in comparison with **OTFP** showing interactions with additional residues of the hydrophobic region including Leu298, Ile304 and Met390. The TFK group shows similar binding in the GVIA iPLA₂ binding site including H-bonding of the oxygen atom with the “oxyanion hole” (Gly197/ Gly198) and interactions of the fluorine atoms with Asn555 and Arg200. This indicated that the potency and selectivity of these compounds mostly depends on the binding of the sulfur atom and hydrophobic chain. Further optimization of the hydrophobic chain will lead to new analogues with improved potency and selectivity in terms of inhibition of GVIA iPLA₂.

3. Conclusion

In this study, beta-thio TFKs containing a hydrophobic chain were identified as potent and selective inhibitors for GVIA iPLA₂. Compound **OTFP** which contains an eight carbon atom alkyl chain exhibited the highest inhibitory activity against the enzyme. This study also showed that the enzyme exhibits a preference for the size of the compound. By combining DXMS with computer-aided design techniques, the binding mode of the **OTFP** inhibitor in the binding site of the enzyme was identified. This is very important since no crystal structure has been solved for the enzyme co-crystallized with inhibitors to assist virtual screening for identifying new potent and selective inhibitors for GVIA iPLA₂. Docking calculations led to the development of structure-activity relationship (SAR) conclusions and gave insight into the binding of these inhibitors. The docking complexes also revealed a detailed binding mode for these inhibitors suggesting that the potency and selectivity can be improved by optimizing the interactions of the hydrophobic chain. In future work, we will employ the SAR to discover new inhibitors for GVIA iPLA₂ as well as to further understand why the enzyme has a preference for small compounds, while its natural substrate consists of relatively large phospholipid molecules. This study will serve as a precursor for developing new potent and selective inhibitors not only for GVIA iPLA₂, but also for GIVA cPLA₂ as well by altering the size and substitutions of the hydrophobic chain. New inhibitors for these two major cellular enzymes will serve as tools to further understand their mechanism of action as well as their biological functions and pathways.

4. Experimental Section

4.1. Enzymatic Assays

4.1.1. Materials—1-Palmitoyl-2-arachidonoyl-*sn*-glycero-3-phosphocholine (PAPC) was purchased from Avanti Polar Lipids, Inc. (Alabaster, Alabama 35007-9105). 1-palmitoyl-2-arachidonoyl-*sn*-glycero-3-phosphocholine (PAPC), [arachidonoyl-1-¹⁴C]-, 10 μ Ci was purchased from PerkinElmer (Akron, OH 44311). Chemicals were purchased from Sigma-Aldrich (St. Louis, MO 63103) and all solvents are from Fisher Scientific (Pittsburgh, PA 15275) unless otherwise stated. Sf9 (*Spodoptera frugiperda*) insect cells and culture medium SF900 III SFM were purchased from Life Technologies (Grand Island, NY 14072 USA). Ni-NTA Agarose was obtained from QIAGEN (Valencia, CA 91355). Econo-Column chromatography columns and Bradford assay kits were obtained from Bio-Rad Laboratories (Hercules, CA 94547).

4.1.2. Trifluoromethylketone (TFK) compounds—The compounds were previously synthesized and purified as described [26, 27].

4.1.3. Expression and purifications of PLA₂s—The human GVIA iPLA₂ and GIVA cPLA₂ were expressed using the Baculovirus Expression Vector System (BEVS) and Sf9 cells as described elsewhere [39]. Sf9 cells were seeded in 1 L shaker flasks containing a suspension culture of 500 mL SF900 III SFM medium, and incubated at 27 °C for 24 h before infection. The cells were infected at density of $\sim 1.5 \times 10^6$ cells/mL with a BEVS containing the cDNA of the N-terminal 6 \times His-tag GVIA iPLA₂ or C-terminal 6 \times His-tag GIVA cPLA₂ at an MOI of 0.1 for 96 h. The cells were harvested by centrifugation (2000 rpm, 5 min, and 4 °C), washed with PBS buffer containing protease inhibitors, and frozen at -80 °C until purification. For purifying GVIA iPLA₂, the cell pellet was resuspended in lysis buffer (25 mM Tris-HCl, 100 mM NaCl, 1 M Urea, 2 mM ATP, 10 mM β -Mercaptoethanol, and protease inhibitors). After a mild sonication (10 seconds “on”/60 seconds “off” repeated for 3 times), the insoluble portion was removed by centrifugation at 13,000 rpm for 1 h. The clear lysate was mixed with Ni-NTA resin, which was previously equilibrated in lysis buffer (1 mL Ni-NTA agarose was gently mixed with 4 mL lysis buffer, centrifuged at 1000 rpm for 1 min, and the supernatant was removed for 3 times), and mixed gently on a rotary shaker at 4 °C for 2 h.

The lysate-Ni-NTA mixture was loaded on a column and washed with the wash buffer (25 mM Tris-HCl, 250 mM NaCl, 2 mM ATP, and 10 mM imidazole). Finally the enzyme was eluted with the elution buffer (25 mM Tris-HCl, 50 mM NaCl, 2 mM ATP, and 250 mM imidazole, and 30% glycerol), and dithiothreitol (DTT) was added to each elution fragment at a final concentration of 5 mM. The concentration of the enzyme was measured using the Bradford assay, and the purified enzyme was stored at -80 °C. GIVA cPLA₂ was purified using the same buffers but without ATP. The final concentration of DTT in the elution fragment was 2 mM, and the enzyme was stored at -20 °C. The human GV sPLA₂ was expressed and purified as previously described by our lab and stored at 4 °C [47].

4.1.4. PLA₂ activity assays—The activity of human GVIA iPLA₂, GIV cPLA₂ and GV sPLA₂ was determined using a group-specific mixed micelle modified Dole assay [33, 34].

The substrate was prepared using slightly different conditions for each enzyme to achieve optimum activity: (i) GVIA iPLA₂ mixed micelle substrate consisted of 400 μM Triton X-100, 98.3 μM PAPC, and 1.7 μM arachidonyl-1-¹⁴C PAPC in a buffer containing 100 mM HEPES pH 7.5, 2 mM ATP, and 4 mM DTT; (ii) GIVA cPLA₂ mixed micelle substrate consisted of 400 μM Triton X-100, 95.3 μM PAPC, 1.7 μM arachidonyl-1-¹⁴C PAPC, and 3 μM PI(4,5)P₂ in a buffer containing 100 mM HEPES pH 7.5, 90 μM CaCl₂, 2 mM DTT, and 0.1 mg/ml BSA; and (iii) GV sPLA₂ mixed micelles substrate consisted of 400 μM Triton X-100, 98.3 μM PAPC, and 1.7 μM arachidonyl-1-¹⁴C PAPC in a buffer containing 50 mM Tris-HCl pH 8.0, and 5 mM CaCl₂. The compounds were initially screened at 0.091 mole fraction (5 μL of 5 mM inhibitor in DMSO) in substrate (495 μL). X_I(50) was determined for compounds exhibiting greater than 93% inhibition. Inhibition curves were generated using GraphPad Prism 5.0 and the non-linear regression by plotting percentage of inhibition vs log (mole fraction) to calculate the reported X_I(50) and its associated error.

4.2. Hydrogen/Deuterium Exchange Mass Spectrometry (DXMS)

4.2.1. Preparation of deuterated samples—For preparing the deuterated samples, deuterium dioxide (D₂O) buffer containing 8.3 mM Tris-HCl (pD of 7.5), 100 mM NaCl in 98% D₂O was used. DXMS experiments were performed according to the previously published method [14, 40]. Briefly, 20 μL of GVIA iPLA₂ (total 40 μg of enzyme) were mixed with 60 μL of D₂O buffer to a final concentration of 73% D₂O. Inhibitor binding experiments were performed incubating first GVIA iPLA₂ with 40 μM of OTFP or DMSO for the control. The final concentration of DMSO was less than 1% for all experiments. The inhibitor was incubated with the enzyme for 30 min at room temperature. D₂O buffer was added to the samples, and they were incubated for an additional 10, 30, 100, 300, 1000, 3000, and 10 000 sec. The final concentration of OTFP, after the addition of D₂O buffer was 10 μM. The deuterium exchange was quenched by adding 120 μL of ice-cold quench solution containing 0.8% formic acid, 2 M guanidine hydrochloride (GdHCl), and 16.6% glycerol that acidified the samples to a final pH of 2.5. The samples were immediately frozen on dry ice, and were stored at -80 °C until analysis (usually within 48 h).

4.2.2. Proteolysis, Liquid Chromatography, and Mass Spectrometry Analysis

For proteolysis and mass spectrometry analysis, the samples were thawed and injected to a pepsin column for digestion as previously described [14, 40]. The proteolytic fragments (peptides) were separated on a C18 reversed phase analytical column at 0 °C. The peptides were analyzed on an OrbiTrap Elite Mass Spectrometer (ThermoFisher Scientific, San Jose, CA). Peptides were analyzed with tandem mass spectrometry (MS/MS) data using SEQUEST (Thermo Finnigan, Inc.). The DXMS Explorer (Sierra Analytics Inc., Modesto CA) was employed to analyze the results and calculate the average of the mass envelope as previously described [14, 38].

4.3. Computer-Aided Drug Design

4.3.1. Induced Fit Docking (IFD) protocol—The GVIA iPLA₂-OTFP initial complexes were generated using the IFD protocol implemented in Schrödinger Suite [41, 48]. The 3D structure of GVIA iPLA₂ (receptor) was prepared and optimized using the Protein Preparation Wizard (PPW) module [44]. Residues Gly486, Gly487, Lys489, Ser519,

Val548, Phe549, Leu560, Tyr643, Phe644, Asp652, Lys729, and Leu770 were selected to define the binding site of GVIA iPLA₂ in the IFD calculations. The inhibitor 3D structures (ligand) were sketched using Maestro 9.9 sketcher, [49] and they were optimized using the LigPrep 3.2 application [50]. IFD protocol employs Glide 6.5 [45] and the refinement module in Prime 3.8 [51] to accurately predict enzyme-inhibitor complexes by incorporating side-chain flexibility for the receptor. The box center for the docking calculations was defined using the centroid of selected residues that were found to constitute the binding site of GVIA iPLA₂ using DXMS and extensive MD simulations in our previously published papers [12-14]. The box size was determined automatically according to the centroid of the specified binding site residues. For the initial docking of the inhibitors the side-chain of the binding site residues were trimmed automatically based on the B-factor. The receptor van der Waals scaling was set to 0.70 and the ligand van der Waals scaling to 0.50. Twenty poses (binding modes) of each inhibitor were allowed to pass to the Prime refinement step. During the Prime refinement step, the side-chains of the residues within 6 Å the inhibitor pose were optimized in terms of conformation and potential energy. Finally, twenty enzyme-inhibitor structures were allowed to pass to the redocking step with a threshold for eliminating high-energy structures from the Prime refinement of 30 kcal/mol, and the Glide Extra-Precision (XP) scoring function [52]. The final complexes were selected based on the binding mode and the score.

4.3.2. Molecular dynamics (MD) simulations—MD simulations were carried on the IFD GVIA iPLA₂-OTFP complex. The complex was placed on a POPC membrane patch of area $\sim 100 \times 100 \text{ \AA}^2$ according to our previously published model [13]. POPC molecules within 0.6 Å of the enzyme were removed, the system was solvated with TIP3P water molecules and sodium chloride at a concentration of 100 mM. The total number of atoms of the entire system was approximately 105,000. NAMD 2.9 was employed for the MD simulations. The CHARMM General Force Field (CGenFF) and parameters were used for the OTFP inhibitor, [53] and the CHARMM36 all-atom additive force field and parameters were used for the enzyme and the POPC membrane patch [54]. The system was minimized for 20,000 steps and equilibrated for 12 ns to relieve all the unfavorable contacts. Finally, a 300 ns MD simulation was performed at a temperature of 310 K using the *NPT* ensemble.

4.3.3. Docking Calculations—Clustering analysis was performed on the trajectories derived from the MD simulations on the enzyme-OTFP complex in order to identify suitable conformations for the docking calculations. The 3D structures were optimized using the PPW [44]. The 3D structures of the inhibitors were sketched using Maestro 9.9 sketcher [49] and they were optimized using LigPrep 3.2 [50]. Glide 5.8 was used for the rigid-docking of the compounds into the enzyme binding pocket [45]. The grid required for the docking procedure was generated using a scaling factor of 1.0 and partial charge cutoff of 0.25, while *X*, *Y*, *Z* dimensions of the inner box were set to 12 Å around the docked inhibitor. For the inhibitor docking a scaling factor of 0.8 and partial charge cutoff of 0.15 were used that allow complete flexibility of the structures. The poses were selected according to the binding mode and the XP GScore. The Glide Extra-Precision (XP) scoring function was used for the calculations [52].

Supplementary Material

Refer to Web version on PubMed Central for supplementary material.

Acknowledgements

This work was supported by NIH Grant GM20501-40 (E. A. D) and by NIH, NSF, NBCR and HHMI (J.A.M). Partial support for this work was received from NIEHS R01 ES002710 and NIEHS Superfund Program P42 ES04699 (B. D. H.). This work used the Extreme Science and Engineering Discovery Environment (XSEDE), which is supported by National Science Foundation grant number ACI-1053575.

References

1. Dennis E, Cao J, Hsu Y-H, Magrioti V, Kokotos G. Phospholipase A₂ enzymes: physical structure, biological function, disease implication, chemical inhibition, and therapeutic intervention. *Chem. Rev.* 2011; 111:6130–6185. [PubMed: 21910409]
2. Mouchlis VD, Dennis EA. Membrane and inhibitor interactions of intracellular phospholipases A₂. *Adv. Biol. Regul.* 2015
3. Buczynski M, Dumlao D, Dennis E. Thematic review series: proteomics. an integrated omics analysis of eicosanoid biology. *J. Lipid Res.* 2009; 50:1015–1038. [PubMed: 19244215]
4. O'Byrne PM. Leukotrienes in the pathogenesis of asthma. *Chest.* 1997; 111:27S–34S. [PubMed: 9042024]
5. Venable ME, Olson SC, Nieto ML, Wykle RL. Enzymatic studies of lyso platelet-activating factor acylation in human neutrophils and changes upon stimulation. *J. Biol. Chem.* 1993; 268:7965–7975. [PubMed: 8463317]
6. Pniewska E, Pawliczak RC. The involvement of phospholipases A₂ in asthma and chronic obstructive pulmonary disease. *Mediators Inflamm.* 2013; 2013:793505. [PubMed: 24089590]
7. Masuda S, Murakami M, Komiyama K, Ishihara M, Ishikawa Y, Ishii T, Kudo I. Various secretory phospholipase A₂ enzymes are expressed in rheumatoid arthritis and augment prostaglandin production in cultured synovial cells. *FEBS J.* 2005; 272:655–672. [PubMed: 15670148]
8. Scott KF, Sajinovic M, Hein J, Nixdorf S, Galetti P, Liauw W, de Souza P, Dong Q, Graham GG, Russell PJ. Emerging roles for phospholipase A₂ enzymes in cancer. *Biochimie.* 2010; 92:601–610. [PubMed: 20362028]
9. Ayilavarapu S, Kantarci A, Fredman G, Turkoglu O, Omori K, Liu H, Iwata T, Yagi M, Hasturk H, Van Dyke TE. Diabetes-induced oxidative stress is mediated by Ca²⁺-independent phospholipase A₂ in neutrophils. *J. Immunol.* 2010; 184:1507–1515. [PubMed: 20053941]
10. Malhotra A, Edelman-Novemsky I, Xu Y, Plesken H, Ma J, Schlame M, Ren MC. Role of calcium-independent phospholipase A₂ in the pathogenesis of Barth syndrome. *PNAS.* 2009; 106:2337–2341. [PubMed: 19164547]
11. Engel LA, Jing Z, O'Brien DE, Sun M, Kotzbauer PTC. Catalytic function of PLA₂G6 is impaired by mutations associated with infantile neuroaxonal dystrophy but not dystonia-parkinsonism. *PLoS One.* 2009; 5:e12897.
12. Mouchlis VD, Bucher D, McCammon JA, Dennis EA. Membranes serve as allosteric activators of phospholipase A₂, enabling it to extract, bind, and hydrolyze phospholipid substrates. *PNAS.* 2015; 112:E516–E525. [PubMed: 25624474]
13. Bucher D, Hsu YH, Mouchlis VD, Dennis EA, McCammon JA. Insertion of the Ca²⁺-independent phospholipase A₂ into a phospholipid bilayer via coarse-grained and atomistic molecular dynamics simulations. *PLoS Comput. Biol.* 2013; 9:e1003156. [PubMed: 23935474]
14. Hsu Y-H, Bucher D, Cao J, Li S, Yang S-W, Kokotos G, Woods V, McCammon J, Dennis E. Fluoroketone inhibition of Ca²⁺-independent phospholipase A₂ through pinding pocket association defined by hydrogen/deuterium exchange and molecular dynamics. *J. Am. Chem. Soc.* 2013; 135:1330–1337. [PubMed: 23256506]

15. Ackermann EJ, Conde-Frieboes K, Dennis EA. Inhibition of macrophage Ca²⁺-independent phospholipase A₂ by bromoenol lactone and trifluoromethyl ketones. *J. Biol. Chem.* 1995; 270:445–450. [PubMed: 7814408]
16. Lio YC, Reynolds LJ, Balsinde J, Dennis EA. Irreversible inhibition of Ca²⁺-independent phospholipase A₂ by methyl arachidonyl fluorophosphonate. *Biochim. Biophys. Acta.* 1996; 1302:55–60. [PubMed: 8695655]
17. Barbayianni E, Stephens D, Grkovich A, Magrioti V, Hsu Y-HH, Dolatzas P, Kalogiannidis D, Dennis EA, Kokotos GC. 2-Oxoamide inhibitors of phospholipase A₂ activity and cellular arachidonate release based on dipeptides and pseudodipeptides. *Bioorg. Med. Chem.* 2009; 17:4833–4843. [PubMed: 19443224]
18. Magrioti V, Nikolaou A, Smyrmiotou A, Shah I, Constantinou-Kokotou V, Dennis E, Kokotos G. New potent and selective polyfluoroalkyl ketone inhibitors of GVIA calcium-independent phospholipase A₂. *Bioorg. Med. Chem.* 2013; 21:5823–5829. [PubMed: 23916152]
19. Kokotos G, Hsu Y-H, Burke J, Baskakis C, Kokotos C, Magrioti V, Dennis E. Potent and selective fluoroketone inhibitors of group VIA calcium-independent phospholipase A₂. *J. Med. Chem.* 2010; 53:3602–3610. [PubMed: 20369880]
20. Pauling L. Molecular architecture and biological reactions. *Chem. Eng. News.* 1946; 24:1375–1377.
21. Brodbeck U, Schweikert K, Gentinetta R. Fluorinated aldehydes and ketones acting as quasi-substrate inhibitors of acetylcholinesterase. *Biochim. Biophys. Acta.* 1979; 567:357–369. [PubMed: 444532]
22. Hammock BD, Wing KD, McLaughlin J, Lovell VM, Sparks TC. Trifluoromethylketones as possible transition state analog inhibitors of juvenile hormone esterase. *Pestic. Biochem. Physiol.* 1982; 17:76–88.
23. Hammock BD, Abdel-Aal YAI, Mullin CA, Hanzlik TN, Roe RM. Substituted thiotrifluoropropanones as potent selective inhibitors of juvenile hormone esterase. *Pestic. Biochem. Physiol.* 1984; 22:209–223.
24. Abdel-Aal Y, Hammock B. Transition state analogs as ligands for affinity purification of juvenile hormone esterase. *Science.* 1986; 233:1073–1076. [PubMed: 3738525]
25. Ashour M-BA, Hammock BD. Substituted trifluoroketones as potent, selective inhibitors of mammalian carboxylesterases. *Biochem. Pharmacol.* 1987; 36:1869–1879. [PubMed: 3593399]
26. Wheelock CE, Colvin ME, Uemura I, Olmstead MM, Sanborn JR, Nakagawa Y, Jones DA, Hammock BD. Use of ab initio calculations to predict the biological potency of carboxylesterase inhibitors. *J. Med. Chem.* 2002; 45:5576–5593. [PubMed: 12459025]
27. Wheelock CE, Severson TF, Hammock BD. Synthesis of new carboxylesterase inhibitors and evaluation of potency and water solubility. *Chem. Res. Toxicol.* 2001; 14:1563–1572. [PubMed: 11743738]
28. Huang TL, Shiotsuki T, Uematsu T, Borhan B. Structure-activity relationships for substrates and inhibitors of mammalian liver microsomal carboxylesterases. *Pharm. Res.* 1996; 13:1495–1500. [PubMed: 8899840]
29. Wogulis M, Wheelock CE, Kamita SG, Hinton AC, Whetstone PA, Hammock BD, Wilson DK. Structural studies of a potent insect maturation inhibitor bound to the juvenile hormone esterase of *Manduca sexta*. *Biochemistry.* 2006; 45:4045–4057. [PubMed: 16566578]
30. Roe RM, Anspaugh DD, Venkatesh K. A novel geminal diol as a highly specific and stable in vivo inhibitor of insect juvenile hormone esterase. *Arch. Insect. Biochem. Physiol.* 1997; 36:165–179.
31. Guthrie PJ. Carbonyl addition reactions: Factors affecting the hydrate-hemiacetal and hemiacetal-acetal equilibrium constants. *Canad. J. Chem.* 1975; 53:898–906.
32. Wadkins RM, Hyatt JL, Edwards CC, Tsurkan L, Redinbo MR, Wheelock CE, Jones PD, Hammock BD, Potter PM. Analysis of mammalian carboxylesterase inhibition by trifluoromethylketone-containing compounds. *Mol. Pharmacol.* 2007; 71:713–723. [PubMed: 17167034]
33. Six DA, Barbayianni E, Loukas V, Constantinou-Kokotou V, Hadjipavlou-Litina D, Stephens D, Wong AC, Magrioti V, Moutevelis-Minakakis P, Baker SF, Dennis EA, Kokotos G. Structure-

- activity relationship of 2-oxoamide inhibition of group IVA cytosolic phospholipase A₂ and group V secreted phospholipase A₂. *J. Med. Chem.* 2007; 50:4222–4235. [PubMed: 17672443]
34. Yang H, Mosior M, Johnson C, Chen Y, Dennis E. Group-specific assays that distinguish between the four major types of mammalian phospholipase A₂. *Anal. Biochem.* 1999; 269:278–288. [PubMed: 10221999]
35. Cao J, Burke J, Dennis E. Using hydrogen/deuterium exchange mass spectrometry to define the specific interactions of the phospholipase A₂ superfamily with lipid substrates, inhibitors, and membranes. *J. Biol. Chem.* 2013; 288:1806–1813. [PubMed: 23209293]
36. Mehmood S, Domene C, Forest E. Dynamics of a bacterial multidrug ABC transporter in the inward-and outward-facing conformations. *PNAS.* 2012; 109:10832–10836. [PubMed: 22711831]
37. West GM, Chien EYT, Katritch V, Gatchalian J. Ligand-dependent perturbation of the conformational ensemble for the GPCR β 2 adrenergic receptor revealed by HDX. *Structure.* 2011; 19:1424–1432. [PubMed: 21889352]
38. Hsu Y-H, Burke J, Li S, Woods V, Dennis E. Localizing the membrane binding region of Group VIA Ca²⁺-independent phospholipase A₂ using peptide amide hydrogen/deuterium exchange mass spectrometry. *J. Biol. Chem.* 2009; 284:23652–23661. [PubMed: 19556238]
39. Burke J, Hsu Y-H, Deems R, Li S, Woods V, Dennis E. A phospholipid substrate molecule residing in the membrane surface mediates opening of the lid region in group IVA cytosolic phospholipase A₂. *J. Biol. Chem.* 2008; 283:31227–31236. [PubMed: 18753135]
40. Burke J, Babakhani A, Gorfe A, Kokotos G, Li S, Woods V, McCammon J, Dennis E. Location of inhibitors bound to group IVA phospholipase A₂ determined by molecular dynamics and deuterium exchange mass spectrometry. *J. Am. Chem. Soc.* 2009; 131:8083–8091. [PubMed: 19459633]
41. Induced fit docking protocol 2014, Glide version 6.5, Prime version 3.8. Schrödinger, LLC; New York, NY: 2014. 2014
42. Phillips J, Braun R, Wang W, Gumbart J, Tajkhorshid E, Villa E, Chipot C, Skeel R, Kalé L, Schulten K. Scalable molecular dynamics with NAMD. *J. Comput. Chem.* 2005; 26:1781–1802. [PubMed: 16222654]
43. Bissantz C, Kuhn B, Stahl M. A medicinal chemist's guide to molecular interactions. *Journal of medicinal chemistry.* 2010; 53:5061–5084. [PubMed: 20345171]
44. Protein preparation wizard 2014-4; Epik version 2.4. Schrödinger, LLC; New York, NY: 2014. Impact version 5.9. Schrödinger, LLC; New York, NY: 2014. Prime version 3.2. Schrödinger, LLC; New York, NY: 2014. 2014
45. Glide, version 6.5. Schrödinger, LLC; New York, NY: 2014. 2014
46. Baskakis C, Magrioti V, Cotton N, Stephens D, Constantinou-Kokotou V, Dennis EA, Kokotos G. Synthesis of polyfluoro ketones for selective inhibition of human phospholipase A₂ enzymes. *J. Med. Chem.* 2008; 51:8027–8037. [PubMed: 19053783]
47. Chen Y, Dennis EA. Expression and characterization of human group V phospholipase A₂. *Biochim. Biophys. Acta.* 1998; 1394:57–64. [PubMed: 9767110]
48. Sherman W, Day T, Jacobson MP, Friesner RA, Farid R. Novel procedure for modeling ligand/receptor induced fit effects. *J. Med. Chem.* 2006; 49:534–553. [PubMed: 16420040]
49. Maestro, version 9.9. Schrödinger, LLC; New York, NY: 2014. 2014
50. LigPrep, version 3.2. Schrödinger, LLC; New York, NY: 2014. 2014
51. Prime, version 3.8. Schrödinger, LLC; New York, NY: 2014. 2014
52. Friesner RA, Murphy RB, Repasky MP, Frye LL, Greenwood JR, Halgren TA, Sanschagrin PC, Mainz DT. Extra precision glide: docking and scoring incorporating a model of hydrophobic enclosure for protein-ligand complexes. *J. Med. Chem.* 2006; 49:6177–6196. [PubMed: 17034125]
53. Vanommeslaeghe K, Hatcher E, Acharya C, Kundu S, Zhong S, Shim J, Darian E, Guvench O, Lopes P, Vorobyov I, Mackerell AC. CHARMM general force field: A force field for drug-like molecules compatible with the CHARMM all-atom additive biological force fields. *J Comput. Chem.* 2009; 31:671–690.
54. Klauda JB, Venable RM, Freites JA, O'Connor JW, Tobias DJ, Mondragon-Ramirez C, Vorobyov I, MacKerell AD, Pastor RWC. Update of the CHARMM all-atom additive force field for lipids: validation on six lipid types. *J. Phys. Chem. B.* 2010; 114:7830–7843. [PubMed: 20496934]

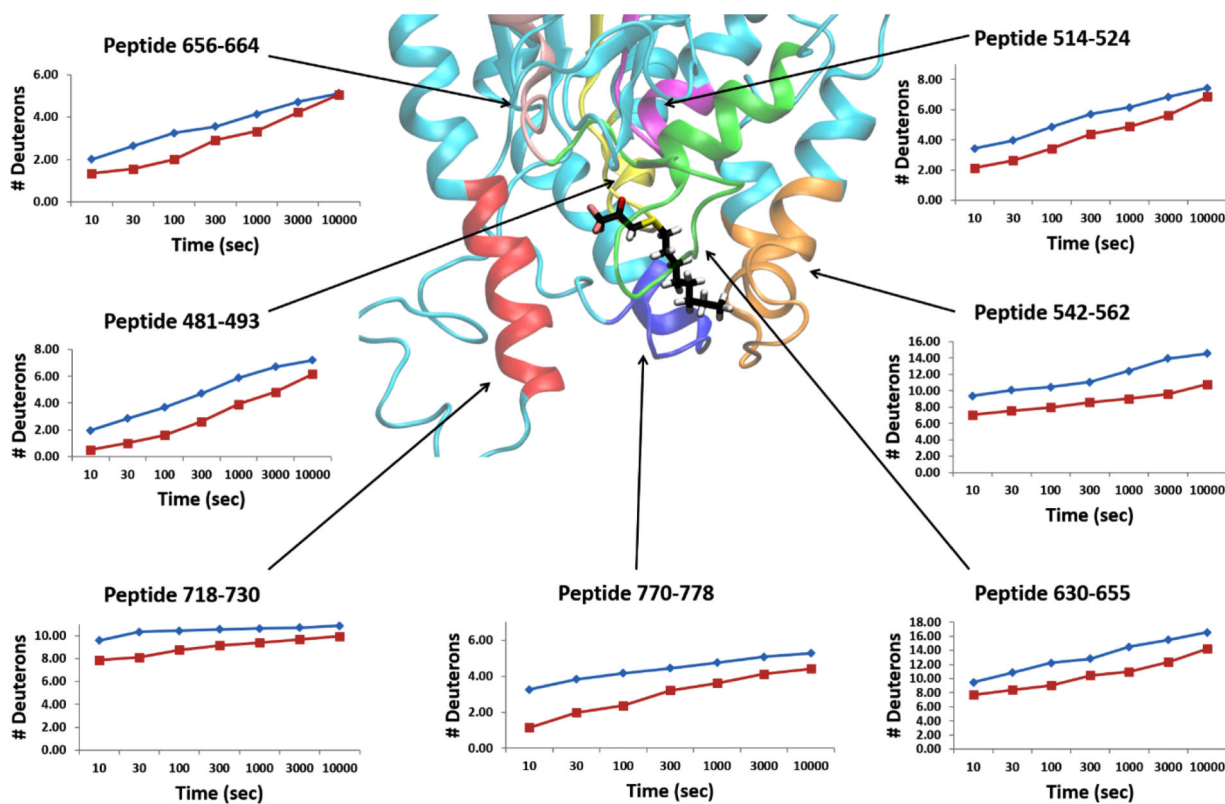


Fig. 1. Hydrogen/Deuterium exchange results upon binding of **OTFP** to GVIA iPLA₂ binding site. Percentage of deuteration level is presented for each peptide region of GVIA iPLA₂ in the absence (blue) and presence (red) of **OTFP**. For each curve seven time points were studied and seven different regions showed a decrease of deuteration rates upon **OTFP** binding: residues 481-493 (yellow), 514-524 (magenta), 542-562 (orange), 630-655 (green), 656-664 (pink), 718-730 (red), and 770-778 (blue).

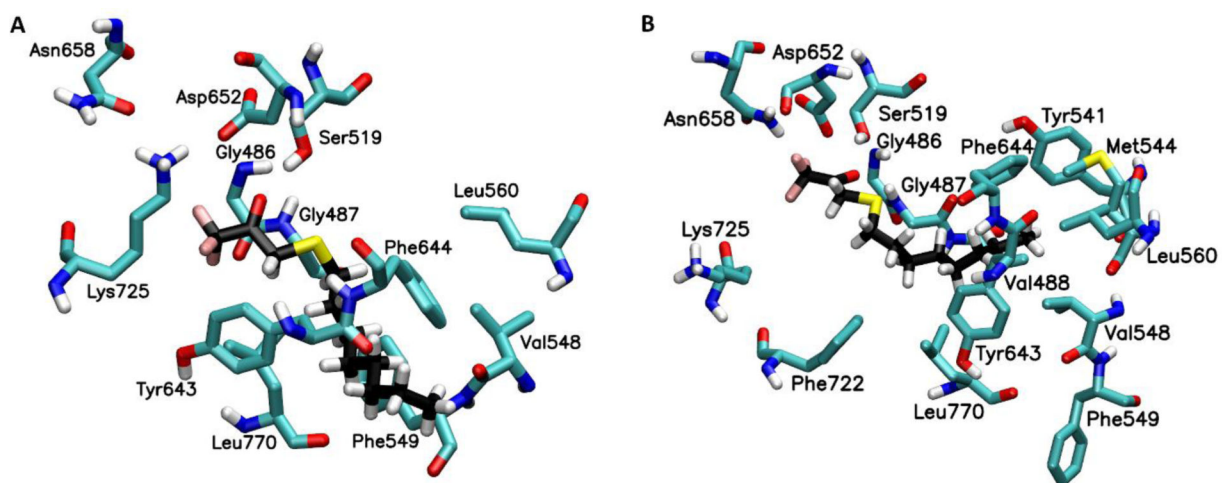


Fig. 2. Binding mode of **OTFP** in the GVIA iPLA₂ binding site. (A) Initial complex generated by IFD. (B) Complex after the MD simulation.

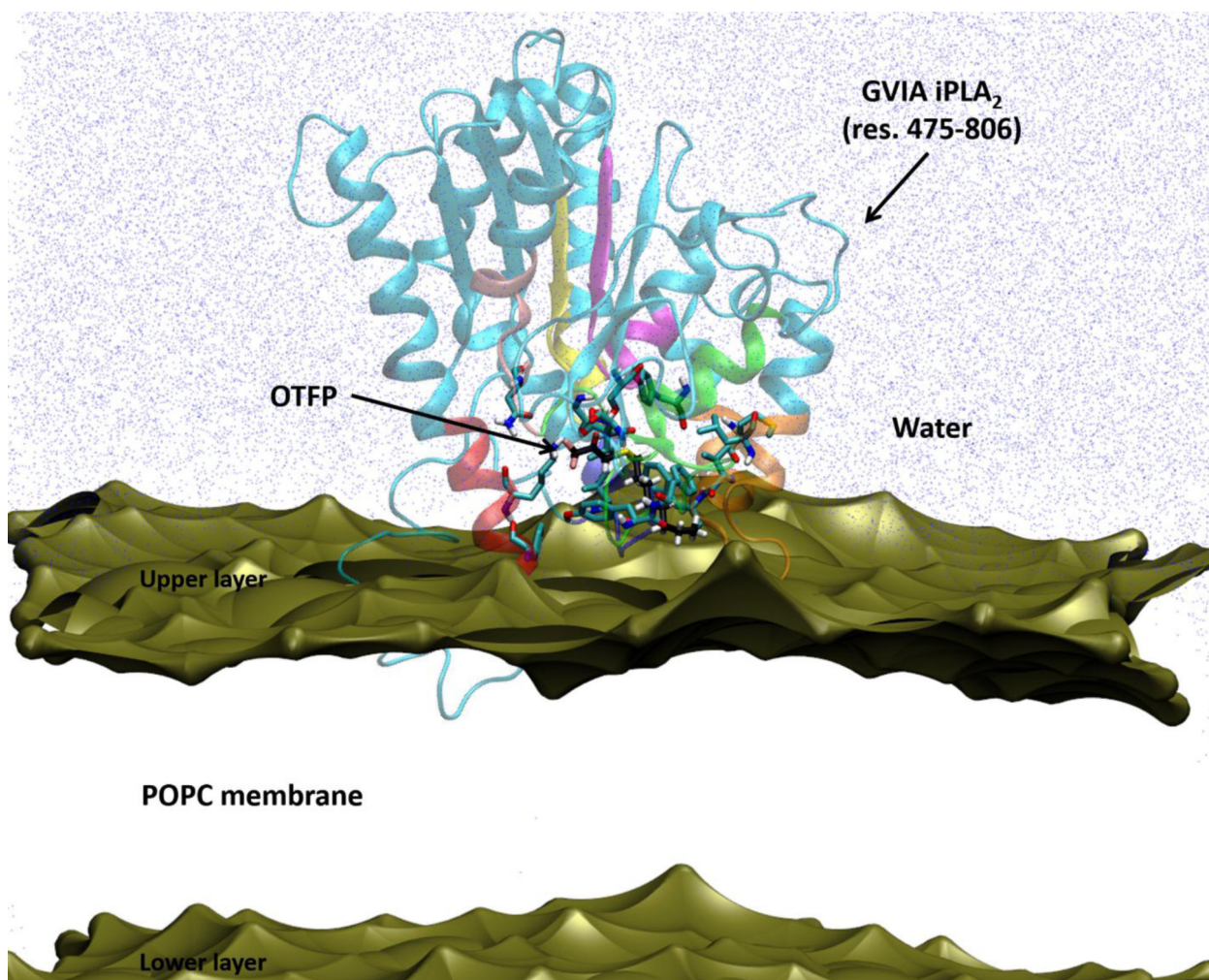


Figure 3.
GVIA iPLA₂-OTFP IFD complex on the surface of a POPC membrane patch and solvated with water molecules.

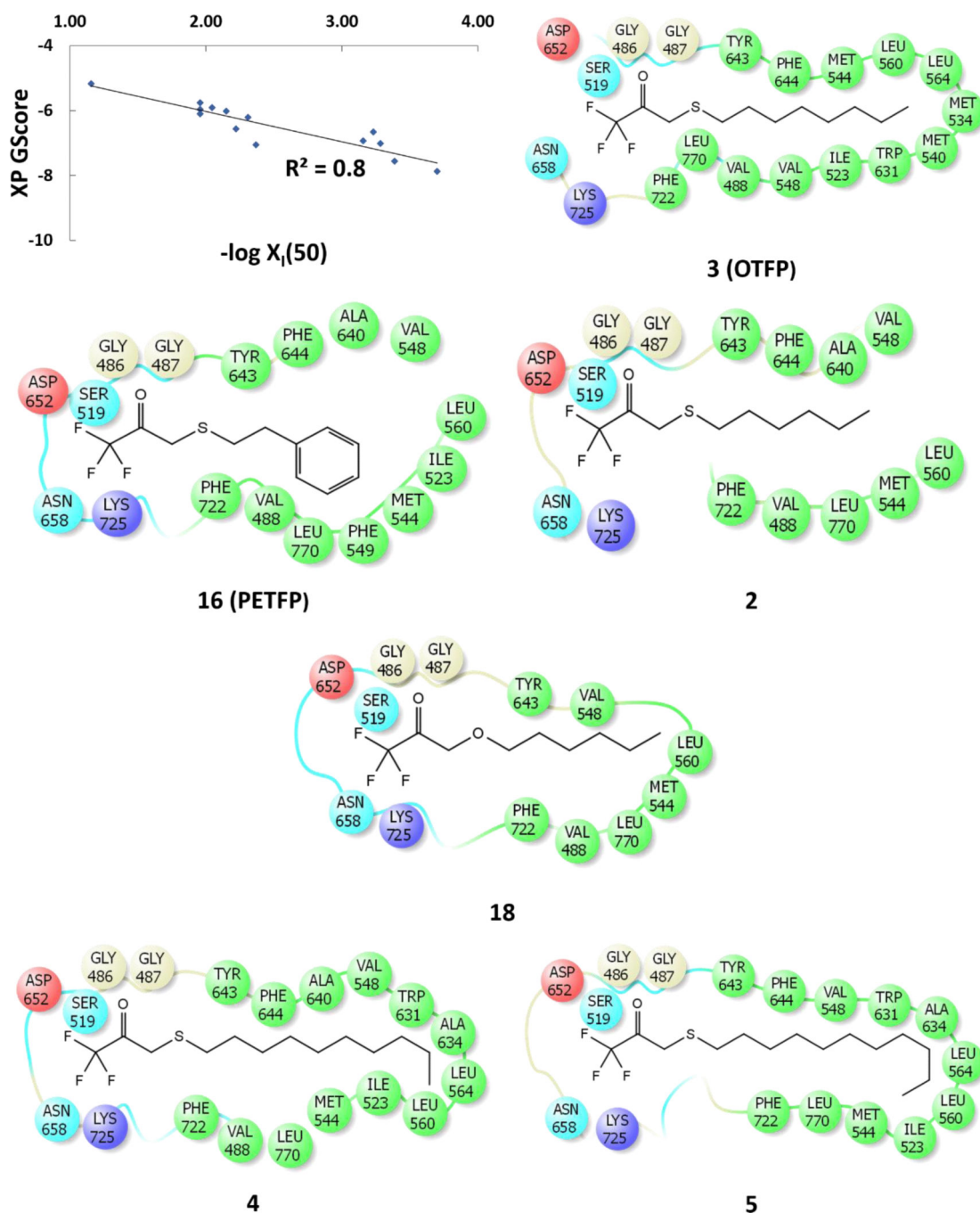


Figure 4. Correlation between theoretical XP GScore vs experimental $-\log X_i(50)$ values and schematic representation of the interactions of representative inhibitors with GVIA iPLA₂ binding site.

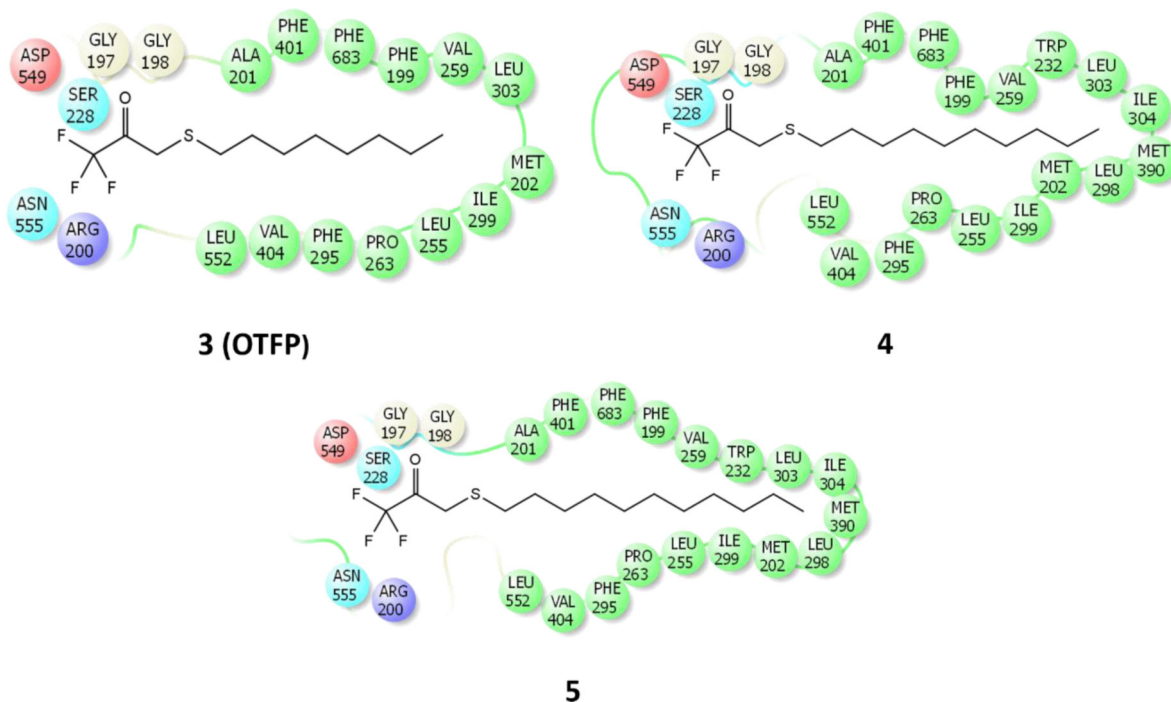
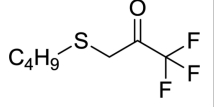
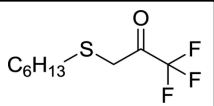
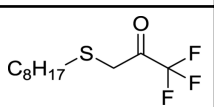
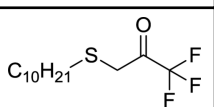
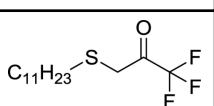
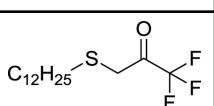
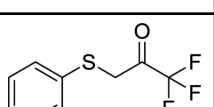
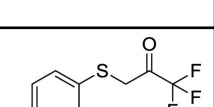
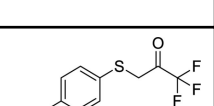
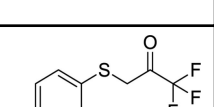
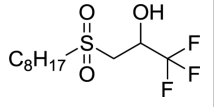
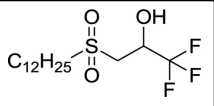
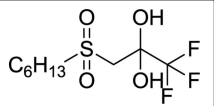
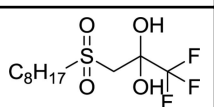
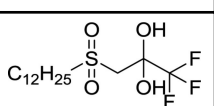


Figure 5.
Schematic representation of the interactions of **OTFP**, **4** and **5** with GIVA cPLA₂ binding site.

Table 1Inhibition of Human GVIA iPLA₂, GIVA cPLA₂, and GV sPLA₂ by TFKs^a

No	Structure	GVIA iPLA ₂		GIVA cPLA ₂		GV sPLA ₂
		% Inhibition	X _I (50)	% Inhibition	X _I (50)	% Inhibition
1		91 ± 1	0.07 ± 0.04	46 ± 7	...	14 ± 12
2		99 ± 1	0.00052 ± 0.00005	77 ± 3	...	33 ± 10
3		99 ± 0.2	0.00020 ± 0.00002	82 ± 1	...	68 ± 3
4		99 ± 0.3	0.00041 ± 0.00003	100 ± 1	0.008 ± 0.001	78 ± 2
5		98 ± 0.2	0.0007 ± 0.0001	98 ± 0.2	0.014 ± 0.002	73 ± 0.4
6		97 ± 0.2	0.0043 ± 0.0009	83 ± 1	...	87 ± 5
7		89 ± 1	...	75 ± 5	...	27 ± 3
8		95 ± 1	0.009 ± 0.001	61 ± 2	...	18 ± 9
9		93 ± 1	0.011 ± 0.002	70 ± 1	...	16 ± 9
10		46 ± 5	...	24 ± 2	...	14 ± 8

No	Structure	GVIA iPLA ₂		GIVA cPLA ₂		GV sPLA ₂
		% Inhibition	X _I (50)	% Inhibition	X _I (50)	% Inhibition
11		95 ± 1	0.011 ± 0.002	82 ± 1	...	23 ± 3
12		97 ± 1	0.0071 ± 0.0007	82 ± 0.4	...	35 ± 4
13		52 ± 3	...	26 ± 4	...	17 ± 5
14		98 ± 1	0.011 ± 0.002	91 ± 1	...	46 ± 4
15		99 ± 1	0.0049 ± 0.0005	91 ± 1	...	43 ± 7
16		100 ± 4	0.00059 ± 0.00005	92 ± 1	...	61 ± 2
17		46 ± 12	...	18 ± 2	...	44 ± 3
18		99 ± 0.2	0.006 ± 0.001	76 ± 5	...	35 ± 5
19		43 ± 3	...	58 ± 9	...	35 ± 7
20		39 ± 8	...	60 ± 4	...	66 ± 4
21		15 ± 8	...	5 ± 5	...	16 ± 9

No	Structure	GVIA iPLA ₂		GIVA cPLA ₂		GV sPLA ₂
		% Inhibition	X _I (50)	% Inhibition	X _I (50)	% Inhibition
22		24 ± 10	...	5 ± 5	...	23 ± 8
23		32 ± 7	...	2 ± 8	...	80 ± 4
24		71 ± 2	...	14 ± 4	...	0 ± 0
25		82 ± 1	...	19 ± 5	...	18 ± 8
26		52 ± 1	...	34 ± 5	...	44 ± 2

^a Average percent inhibition and standard error (n = 3) are reported for each compound at 0.091 mole fraction. X_I(50) values were determined for inhibitors with greater than 95% inhibition, except for compound **1** which was included in the SAR.

Table 2

Average percentage of deuteration level of the peptide regions that showed decreased exchange rates upon binding with OTFP.

Peptide Region	Average % Deuteration (absence of OTFP)	Average % Deuteration (Presence of OTFP)	Average % Deuteration
481-493 (yellow)	43	27	16
514-524 (magenta)	61	48	13
542-562 (orange)	69	51	18
630-655 (green)	60	48	12
656-664 (pink)	61	49	12
718-730 (red)	95	82	13
770-778 (blue)	63	43	20

Author Manuscript

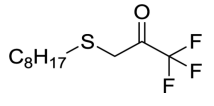
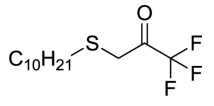
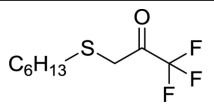
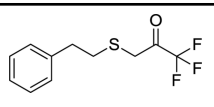
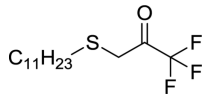
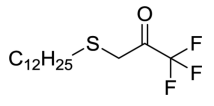
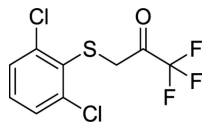
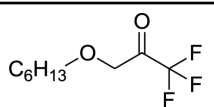
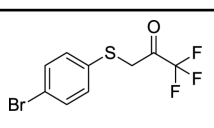
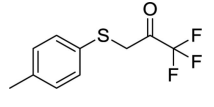
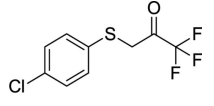
Author Manuscript

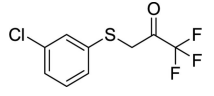
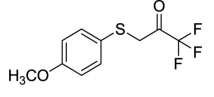
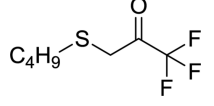
Author Manuscript

Author Manuscript

Table 3

TFKs employed to generate SAR.

No	Structure	$-\log X_I(50)$	XP GScore (GVIA iPLA ₂)	XP GScore (GIVA cPLA ₂)
3		3.7	-7.9	-4.9
4		3.4	-7.6	-6.0
2		3.3	-7.0	...
16		3.2	-6.6	...
5		3.2	-6.9	-5.9
6		2.4	-7.1	...
15		2.3	-6.2	...
18		2.2	-6.6	...
12		2.2	-6.0	...
8		2.1	-5.9	...
11		2.0	-6.1	...

No	Structure	$-\log X_1(50)$	XP GScore (GVIA iPLA ₂)	XP GScore (GIVA cPLA ₂)
14	 <chem>Clc1ccc(cc1)SCC(=O)C(F)(F)F</chem>	2.0	-5.9	...
9	 <chem>COc1ccc(cc1)SCC(=O)C(F)(F)F</chem>	2.0	-5.7	...
1	 <chem>CCCCSCC(=O)C(F)(F)F</chem>	1.2	-5.2	...

Author Manuscript

Author Manuscript

Author Manuscript

Author Manuscript